Mon. Not. R. Astron. Soc. **000**, 000–000 (1999)

Depth of excitation and reversal of asymmetry of low-l solar p modes: a complementary analysis of BiSON * and VIRGO/SPM † data

W. J. Chaplin[1,2‡] & T. Appourchaux[1§]
[1] *ESA Space Science Department, Solar System Division, ESTEC, 2200 AG Noordwijk, The Netherlands.*
[2] *School of Physics and Astronomy, University of Birmingham, Edgbaston, Birmingham B15 2TT, U.K.*

7 July 1999

ABSTRACT

We use the solutions to a simple, one-dimensional wave equation – which is intended to describe the essential elements of the solar resonant acoustic cavity – as formalistic models to which to fit low-l modes in observational helioseismic power spectra. We have analyzed data collected in velocity, by the ground-based Birmingham Solar-Oscillations Network (BiSON), and in intensity, by the full-disc VIRGO Sun photometers (SPM) on board the ESA/NASA SOHO satellite.
Our analysis extracts, as a function of the modal radial overtone number n, direct estimates of: the location of the excitation source of the acoustic resonances; and the size of that component of the convective granulation that is correlated to the observations of the resonances, and is responsible for the reversal of asymmetry of the mode profiles when different observation techniques are applied (i.e., intensity or Doppler velocity measurements). This information is coded in the complicated forms of the observed, resonant profiles.

Key words:
methods: data analysis – Sun: oscillations – Sun: interior

1 INTRODUCTION

The presence of skew symmetry in the observed resonant profiles of the solar acoustic modes has now been well established observationally, most recently at low angular degrees (Toutain et al. 1998; Chaplin et al. 1999). It arises because the excitation source is spatially localized with respect to the bounded, resonant cavity in which the modes are formed. The precise nature of the profiles depends critically upon the manner in which the oscillations are observed. Acoustic modes studied in data collected from intensity and Doppler-velocity observations of the visible solar disc usually display opposite signs of asymmetry (Duvall et al. 1993; Toutain et al. 1997; Appourchaux et al. 1998). In order to achieve this reversal, the modifying influence of a noise component that is separate from – but nevertheless correlated with – the observed oscillations is required. Current proposals suggest the granular motion as the source, although specifics regarding which particular aspect of the motion is responsible do differ (Roxburgh & Vorontsov 1997; Nigam et al. 1998; Kumar & Basu 1999a, b).

The implied complexity of the resonant p-mode profiles requires the development of new, more-appropriate techniques of analysis for fitting observational helioseismic power spectra. The motivational reasons for doing this are clear. Analysis methods that allow for skew-symmetric mode shapes will clearly provide more-reliable estimates of the mode parameters themselves. This is particularly true with regard to the eigenfrequencies, since the inappropriate use of symmetric fitting models gives rise to appreciable systematic errors in their estimation (e.g., see Rhodes et al. 1997; Korzennik 1998; Rosenthal 1998a, b; Christensen-Dalsgaard et al. 1998; Toutain et al. 1998; and Chaplin et al. 1999). Further, the imaginative use of new techniques will allow helioseismologists to take advantage of the extra information afforded by the presence of such subtle effects in the data. Here, we do so by applying a new fitting model that returns directly information regarding the excitation of the modes and the manner in which they interact with their

* BiSON URL: http://bison.ph.bham.ac.uk/
† VIRGO URL: http://virgo.so.estec.esa.nl/
‡ e-mail: wchaplin@so.estec.esa.nl
§ e-mail: thierrya@so.estec.esa.nl

environment in the region where the excitation occurs. This information is "coded" in the observed shape of the resonant p-mode spectrum (e.g., see Gabriel 1995; Rast & Bogdan 1997; Nigam et al. 1998; Rosenthal 1998a).

We have used the solutions derived from a simple one-dimensional wave-equation as models to which to fit the low-l resonant peaks in the frequency domain. Wave equations of this type are considered in detail by, for example, Abrams & Kumar (1996), Nigam & Kosovichev (1998) and Kumar & Basu (1999a). We have analyzed independent spectra, generated from observations of the oscillations made in both velocity and intensity. These data were collected by: the ground-based Birmingham Solar-Oscillations Network (BiSON), and the full-disc VIRGO Sun photometers (SPM) on board the ESA/NASA SOHO satellite, respectively. Owing to their explicit presence in the fitting formalism, estimates of the position of the excitation source and the size of the correlated granular component have been extracted directly by the fitting procedures.

2 FITTING MODEL

The solar acoustic cavity is defined in the form of a rectangular potential well, $\Phi(r)$, of width r_a. $\Phi(r)$ takes infinite values beneath the lower turning point of the cavity (which is located at radius $r = 0$) and a constant, finite value above the upper turning point (at $r = r_a$). The wave equation describing this system takes the form:

$$\frac{d^2}{dr^2}\Psi + [\omega^2 + i\Gamma\omega - \Phi(r)]\Psi = S\delta(r - r_s). \tag{1}$$

In the above: Ψ is proportional to the Lagrangian pressure perturbation; Γ measures the damping rate; and the system is excited by a δ-function source with amplitude S located at radius $r = r_s$¶. Clearly, Equation 1 is a somewhat simplified representation of the real solar acoustic cavity. However the resonant profiles given by determining the response of this system to a sudden impulse, i.e., by computing the Green's function G_Ψ for Equation 1, serve to illustrate the skew-symmetric form of the observed solar acoustic resonances. Furthermore, they are sufficiently tractable to be used as formalistic models for mode-fitting procedures.

We define the location of the source with respect to the bounded cavity according to $d_s = r_s - r_a$. When d_s is negative, i.e., for the source inside the cavity, one derives (e.g., Abrams & Kumar 1996):

$$G_\Psi^{\rm in}(\omega_1) = -\frac{\sin(\omega_1 r_s)}{\omega_1\cos(\omega_1 r_a) + \omega_2\sin(\omega_1 r_a)}, \tag{2}$$

where $\omega_1^2 = (\omega^2 + i\omega\Gamma)^2$ and $\omega_2^2 = \omega_c^2 - \omega_1^2$. We have set $\nu_c = \omega_c/2\pi$, the acoustic cut-off frequency, to 5.5 mHz throughout our analyses. (Note that the acoustic potential $\Phi(r) = \omega_c^2$ for $r > r_a$.)

With the source located outside the cavity (i.e., for d_s positive) we have (Kumar & Basu 1999a):

¶ Note that all radii are defined in the form of seconds of travel time.

$$\begin{aligned} G_\Psi^{\rm out}(\omega_1) \quad = \quad & -\frac{\omega_2\sin(\omega_1 r_a)\cosh(\omega_2 d_s)}{\omega_2[\omega_1\cos(\omega_1 r_a) + \omega_2\sin(\omega_1 r_a)]} \\ & -\frac{\omega_1\cos(\omega_1 r_a)\sinh(\omega_2 d_s)}{\omega_2[\omega_1\cos(\omega_1 r_a) + \omega_2\sin(\omega_1 r_a)]}. \end{aligned} \tag{3}$$

Since $G_\Psi^{\rm in}$ and $G_\Psi^{\rm out}$ and their derivatives are continuous at $d_s = 0$ (when $r_s = r_a$), we can establish a composite solution:

$$G_\Psi = \begin{cases} G_\Psi^{\rm in} & \text{for } d_s \leq 0 \\ G_\Psi^{\rm out} & \text{for } d_s > 0 \end{cases} \tag{4}$$

It is now believed that the addition of a correlated noise component $\alpha_{\rm corel}$ to the complex G_Ψ is responsible for reversing the mode asymmetries in the observed power spectrum, and that this arises from the convective motions which excite the acoustic resonances. Here, we follow Kumar & Basu (1999a) in assuming that the velocity observations of the modes are essentially uncorrupted by this granular contribution. Hence, for the BiSON Doppler-velocity observations analyzed in this paper, we set $\alpha_{\rm corel} = 0$. We accept that the assumption of a complete lack of any contamination of the velocity signal is questionable. Nevertheless, the size of any "imprinted" signal present may be somewhat smaller than that observed in intensity. For example, the ratio of the typical magnitude of the velocity and intensity fluctuations associated with the acoustic modes is of the order of $\delta v_{\rm osc}/\delta I_{\rm osc} \sim 50\,{\rm km\,s^{-1}}$ per unit change in intensity; however, the corresponding quotient associated with convective motions at the top of the convection zone is of the order of $\delta v_{\rm con}/\delta I_{\rm con} \sim 10\,{\rm km\,s^{-1}}$ per unit change in intensity (e.g, from observations made by Espagnet et al. 1995; simulations made by Stein & Nordlund 1998). Given these values, the ratio of the size of convective and acoustic disturbances in intensity (i.e., $\delta I_{\rm con}/\delta I_{\rm osc}$) is some ~ 5 times larger than that in velocity (i.e., $\delta v_{\rm con}/\delta v_{\rm osc}$). We might therefore reasonably expect the observations made in intensity to be more prone to contamination by the effects of convection. So, if we accept the premise, a resonant peak in the BiSON spectrum is assumed to take the form:

$$P_{G_\Psi}(\omega) = A_{\rm V}^2 \cdot |G_\Psi^{'}|^2. \tag{5}$$

Here, $G_\Psi^{'}$ is the Green's function, normalized to its maximum value, and $A_{\rm V}$ is the amplitude of the mode to be fitted. For the VIRGO/SPM intensity data, we assume a non-zero $\alpha_{\rm corel}$. A resonant peak in the intensity spectrum then takes the form:

$$P_{G_\Psi}(\omega) = A_{\rm I}^2 \cdot |G_\Psi^{'} + \alpha_{\rm corel}|^2. \tag{6}$$

Owing to the normalization of the Green's function in the fitting, $\alpha_{\rm corel}$ therefore represents that fraction of the maximum value of G_Ψ that is needed to generate the required profile. The effective amplitude of the correlated signal, $A_{\rm corel}$, can be calculated from:

$$A_{\rm corel} = A_{\rm I} \cdot \alpha_{\rm corel}. \tag{7}$$

At this point we note that – for the fitting – we have neglected to include the pre-factor that usually appears in Equations 2 and 3. This modifies G_Ψ according to the radial coordinate at which "observations" of the modes are made (e.g., see Abrams & Kumar 1996; Kumar & Basu 1999a), and serves principally to reflect the exponential attenuation of the resonant signal that results from the point of observation lying in the evanescent region. This is taken care of in the fitting (i.e., the strength or height of each mode is a freely-fitted parameter in the analysis). Further, we have not addressed the issue of the phase relationship of the correlated component and the resonant acoustic signal – here, we have fitted $\alpha_{\rm corel}$ as a real, not a complex, variable (although it is, of course, added in complex manner to the complex elements of G_Ψ).

Our analyses also make use of the fact that the effect of different multipole sources can be treated mathematically, by differentiating G_Ψ with respect to radius. The generation of acoustic noise by turbulent motions was first outlined by Lighthill (1952), and expanded upon for the solar case by, for example, Goldreich & Kumar (1990). Various multipole sources contribute to the generated power: "monopole" radiation arising from the periodic contraction and expansion of an eddy; "dipole" radiation from the displacement of an eddy by an acting force; and "quadrupole" radiation from turbulent Reynolds stresses. The relative contribution of these terms to the excitation of solar p modes is still open to debate, largely as a result of the current lack of a complete theory of convection. In this paper, we shall consider profiles calculated from G_Ψ and its first derivative, dG_Ψ/dr. We have resisted the temptation to describe either as being characterized by a monopole, dipole or quadrupole source, i.e., we do not wish the use of particular mathematics to imply a direct one-to-one correspondence with a particular physical mechanism (also see Rosenthal 1998a for a discussion of this point). However, we note that Kumar & Basu (1999b) match a "dipole" source to profiles generated from G_Ψ, and a "quadrupole" source to those calculated from dG_Ψ/dr.

3 PROPERTIES OF MODELLED PROFILES

Fig. 1 shows the re-normalized real (solid line) and imaginary (dashed line) parts of G_Ψ, simulating an $n = 21$ radial mode. This profile was computed from Equation 2 with a chosen cavity size of $r_a = 3430.5$ sec, a relative source depth of $d_s = -20$ sec (i.e., source lying inside the bounded resonant cavity) and a line width of $1\,\mu$Hz. The real part of the Green's function has a "dispersive" form: it is the vertical displacement, or offset, of this part of the function that gives rise to skew symmetry in the final profile. This can result from either: the introduction of an additional correlated component (e.g., that part of the granular noise that is assumed to imprint itself on the observations of the acoustic modes); or changes to the position of the source with respect to the outer bound of the cavity and its nodes. Physically, the changing skewness resulting from the latter can be understood in terms of phase shifts between acoustic rays which follow different paths emanating from the source, and which ultimately contribute to the observed interference signal.

Let $r_{\rm low}$ to be the peak (or minimum) amplitude of the real part of the function on the low-frequency side of the resonance, and $r_{\rm high}$ be the peak (or minimum) amplitude on the high side. We can then define (for illustrative purposes only) a "skewness" factor according to the normalized ratio:

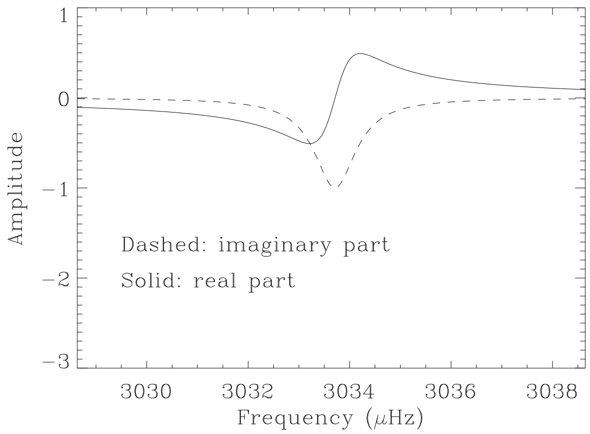

Figure 1. The re-normalized real (solid line) and imaginary (dashed line) parts of G_Ψ, simulating an $n = 21$ radial mode. The profile was computed from Equation 2 with: a cavity size $r_a = 3430.5$ sec; a relative source depth $d_s = -20$ sec; and a line width of $1\,\mu$Hz.

$$\mathcal{F}_{\rm skew} = \frac{r^2_{\rm high} - r^2_{\rm low}}{r^2_{\rm high} + r^2_{\rm low}}.$$

In Fig. 2, we show the variation of $\mathcal{F}_{\rm skew}$ as a function of the source position d_s, for cavities with different properties. We do so for two source "types" – the solid line for a source characterized by G_Ψ; and the dotted line for a source characterized by dG_Ψ/dr (see Section 2). Panel (a) displays the results for a simulated $l = 0$, $n = 10$ mode (at $\sim 1548.3\,\mu$Hz) with cavity size $r_a = 3200$ sec, and damping equivalent to a line width of $0.07\,\mu$Hz; panel (b) those for an $l = 0$, $n = 17$ mode (at $\sim 2496.2\,\mu$Hz) with cavity size $r_a = 3375$ sec, and line width of $0.85\,\mu$Hz; and (c) those for an $l = 0$, $n = 22$ mode (at $\sim 3168.6\,\mu$Hz) with cavity size $r_a = 3441$ sec, and line width of $1.41\,\mu$Hz.

The general features of the plots can be explained as follows. When the source lies inside the cavity, the degree of skew-symmetry increases as the source approaches a node or antinode (depending upon the parity of the source type). The nodal separation of the cavity is determined by the ratio of r_a and the radial overtone number, n, e.g., for the $n = 10$ cavity in panel (a), the separation is ~ 320 sec. The sign of the asymmetry reverses as the source passes through a node or antinode. The asymmetries for the "G_Ψ" source are shifted in phase with respect to those for the "dG_Ψ/dr" source by half the nodal separation. This means that the observed asymmetries are always of opposite sign.

4 DATA

We have fitted the low-l resonant peaks in a 32-month power spectrum, generated from Doppler-velocity residuals collected by BiSON between 1994 May 16 and 1997 Jan 10. In addition, we have also analyzed two spectra generated from data collected by the full-disc VIRGO Sun photometers (SPM) on board the ESA/NASA SOHO satellite. These intensity data – collected at blue (402 nm) and red (862 nm)

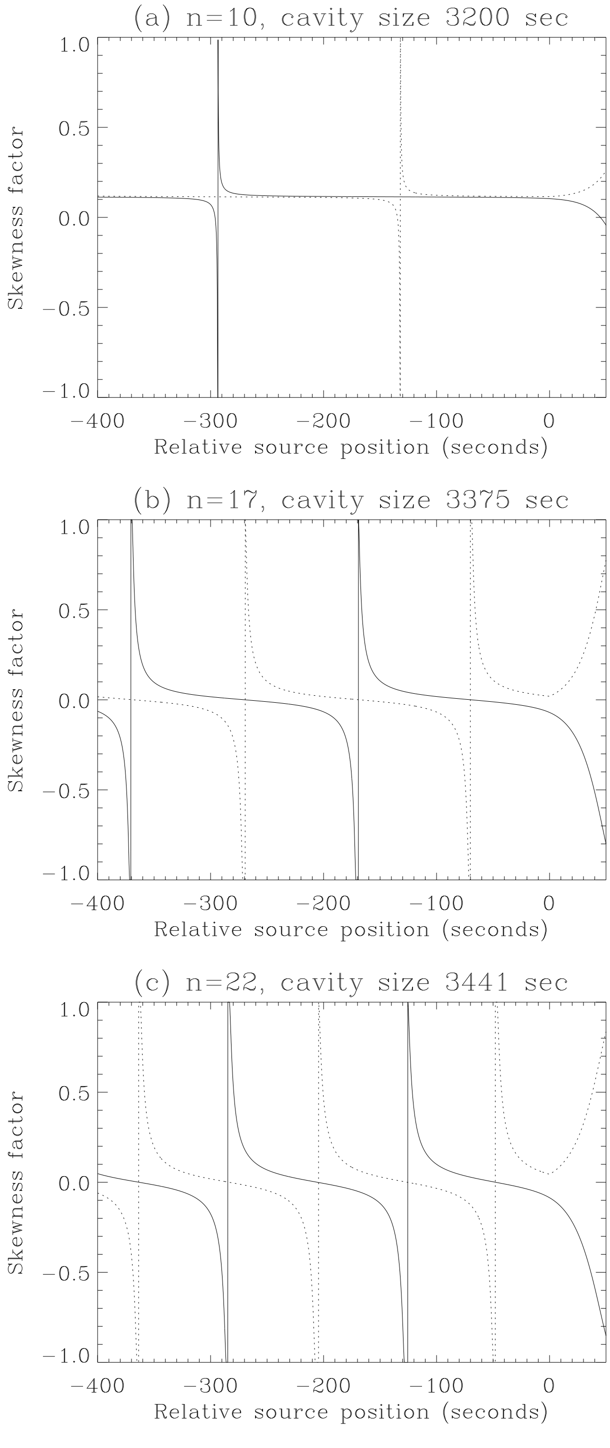

Figure 2. Variation of the skewness factor, $\mathcal{F}_{\rm skew}$, plotted as a function of the source depth, d_s, for different cavity types. The solid line indicates the results for a source, as characterized by G_Ψ, and the dotted line those for a source characterized by dG_Ψ/dr. In (a) – simulated $l = 0$, $n = 10$ mode (at $\sim 1548.3\,\mu$Hz) with cavity size $r_a = 3200\,$sec, and damping equivalent to a line width of $0.07\,\mu$Hz; in (b) – $l = 0$, $n = 17$ mode (at $\sim 2496.2\,\mu$Hz) with cavity size $r_a = 3375\,$sec, and line width of $0.85\,\mu$Hz; and in (c) – $l = 0$, $n = 22$ mode (at $\sim 3168.6\,\mu$Hz) with cavity size $r_a = 3471\,$sec, and line width of $1.41\,\mu$Hz.

wavelengths – cover the period 1996 May 1 through 1997 December 9.

While the BiSON and VIRGO/SPM spectra are not contemporaneous, they both span similar levels of solar activity (i.e., at or near the solar activity cycle 22/23 minimum). We have determined the mean, smoothed (71-d moving mean) 10.7-cm radio flux (in RF units) over the period of both sets of observations. This measure serves as a useful proxy of the level of solar activity. We find the same mean level of ≈ 76 RF units in each case – this should be compared with the notional minimum activity level of 65 RF units. Any concerns regarding comparative errors introduced by differing levels of activity in the BiSON and VIRGO/SPM data can therefore be largely disregarded, although the effects of realization noise may still affect the fits. (For a more in-depth discussion of the issues relating to the comparison of independent helioseismic data, see Chaplin et al. 1998.)

5 RESULTS

5.1 Fitting the BiSON spectrum for the source depth

We have fitted the BiSON Doppler-velocity spectrum to the wave-function model in order to extract estimates of the source depth, d_s, under the premise that G_Ψ is uncorrupted by the granular contribution α_{corel}. Therefore, each peak in the frequency domain is modelled according to Equation 5.

We used a multidimensional direction-set minimization algorithm (Press et al. 1992) to fit adjacent $l = 2/0$ pairs, by maximizing a log-likelihood function commensurate with the assumed negative exponential statistics in the frequency domain. The following parameters were varied iteratively until they converged to their best-fit values:

(i) A cavity travel time, r_a, for each mode in the pair. The first-guess cavity time was chosen to be appropriate to the radial overtone number of each mode, n.
(ii) A single parameter describing the relative source position d_s, i.e., this was assumed to take the same value for each mode in the pair. This is a valid approximation, since the properties of the modes in the near surface layers are essentially independent of l. For this reason – in addition to encouraging stability in the fits by keeping the number of freely varying parameters to a minimum – we have fitted a single parameter only.
(iii) A single parameter describing a symmetric rotational splitting pattern for each mode (not applicable to radial modes). For $n > 24$ the rotational splitting pattern was fixed for all modes, with a constant synodic spacing (appropriate to $\Delta|m| = 1$) of 400 nHz.
(iv) A single width for the pair (i.e., all m components in the pair were assumed to have the same width).
(v) A single height – that of the outer, sectoral m components – for each mode. The relative m-component height ratios were assumed to take fixed values (Christensen-Dalsgaard 1989).
(vi) A flat, background offset for the whole fit.

The relative, temporal sideband heights were fixed at all n according to the characteristics of the window function. These arise from leakage due to the presence of quasi-periodic dataset gaps in the time domain. The natural logarithm of the amplitude, width and background terms were varied – not the straight forward parameters themselves – in order to give a quasi-normal fitting distribution (Toutain & Appourchaux 1994). Estimates of the formal uncertainties in each parameter could then be determined from the inverse of the Hessian matrix describing the hyper-surface of the fit. In Fig. 3, we show the fitted relative source positions d_s, plotted as a function of the overtone number, n, of the radial mode in each fitted pair. Negative values of d_s imply that the source lies inside the bounded cavity. Clearly, for n less than roughly 16, the fits imply that the oscillations are evanescent at the source; for $n > 16$, the source lies just inside the cavity.

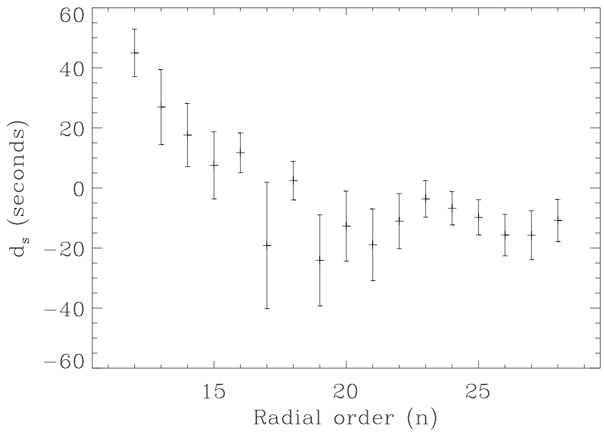

Figure 3. Fitted relative source position, d_s (in seconds of travel time), plotted as a function of the overtone number, n, of the radial mode in each fitted pair. Negative values imply that the source lies inside the resonant cavity. The plotted error bars are the formal uncertainties derived from the Hessian of each fit.

We have tested and validated the fitting procedure by performing an extensive series of Monte Carlo simulations. Many artificial mode pairs were generated, through the use of Equation 4, over a range of simulated n matching that fitted in the real data. We varied the input characteristics to each mode pair (e.g., cavity travel times, splittings, widths, S/N etc.) in order to mimic those present in the BiSON observations. The relative source locations were fixed according to a smooth function fitted through the estimates in Fig. 3. Independent realizations, at each (l, n), of the same basic "limit" pair were generated by applying Gaussian noise in the frequency domain to yield the real and imaginary parts. Each resulting power spectrum was then fitted, as itemized above, and fitted parameter distributions established at each (l, n). From these, we verified the robustness of the source depths and associated uncertainties displayed in Fig. 3.

The relative source locations in Fig. 3 have been converted to absolute heights beneath the base of the photosphere: we have defined this where optical depth reaches unity at 500 nm. To do this, we have used the cavity acoustic potential determined from a solar model (model 'S' of Christensen-Dalsgaard et al. 1996) in order to relate the outer bound of each fitted "cavity" to a physical height in the outer atmosphere of the Sun. The implied absolute

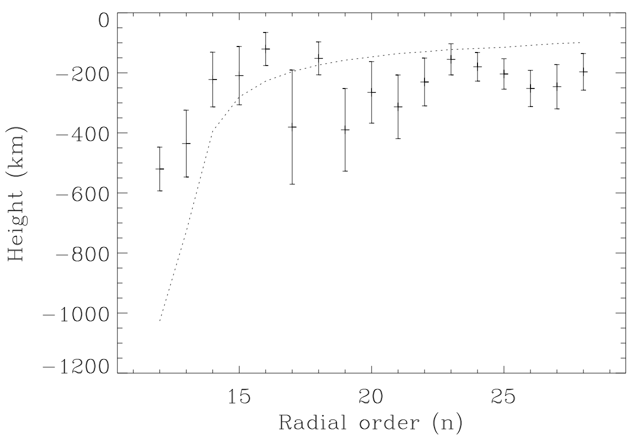

Figure 4. Implied absolute location of the source, in km, beneath the base of the photosphere (defined where optical depth reaches unity at 500 nm). The dotted line indicates the location of the upper turning point of the bounded, resonant cavity for radial modes.

depths are shown in Fig. 4. The dotted line on the figure indicates the location of the upper turning point of the acoustic cavity for radial modes. The (weighted) mean location of the source is -221 ± 17 km, i.e., in the outer layers of the convection zone. These data also suggest a weak frequency dependence, with lower-n modes excited at slightly larger depths. Abrams & Kumar (1996) point out that such behaviour is expected from theories of acoustic noise generation based on turbulent convection and standard mixing length theories, owing to the stratification of eddy scales with height.

Once more, we note that the relative and absolute depths in Figs. 3 and 4 have been obtained under the premise that the BiSON Doppler velocity observations are uncorrupted by any granular contribution, an assumption that is questionable. The presence of such a signature would demand shallower source depths to give the required level of asymmetry (cf. Fig. 2). The plotted data should therefore strictly be regarded as lower-limit estimates of the source location. We tested the effect of the modifying influence of an α_{corel} of size 1 per cent on artificial data generated from G_Ψ. From these, we estimate that were a similar α_{corel} to be present in the BiSON data at all n, the relative source locations d_s would be raised by about 2 sec at the extreme fitted n, and ~ 8 sec near the centre of the 5-minute envelope.

With reference to Fig. 2, one can see that fitting to a function defined by dG_Ψ/dr will yield deeper estimates of the location of the source. For example, with the source placed inside the cavity, its depth is effectively increased by half the cavity-node separation. In fact, we find an implied mean depth over the n range analyzed here of ~ -1500 km. Further, since the node separation is larger at small n, the frequency dependence in the source depth is more pronounced in the dG_Ψ/dr fits.

The interpretation of the depths extracted by the fitting must be approached with a little caution. This is because – as indicated by Fig. 2 – source depths that give similar levels of asymmetry recur throughout the cavity. The fitted values are, therefore, not unique. A similar pattern of skewness values will be replicated by moving each of the fitted relative source-depth estimates shown in Fig. 3 deeper by an amount corresponding to the separation of one cavity node at each n. Since the cavity-node separation is a linear function of n – changing from about 272 to 124 sec over the radial-order range fitted here – the source-depth estimates obtained by moving through one (or more) nodes would display a more-pronounced variation with n, in addition to being noticeably deeper. In fact, we find that as a result of jumping through a single node, the implied absolute source depths would be ≈ -3000 km at $n \sim 12$, and ≈ -1700 km at $n \sim 28$. The disparity between the low- and high-n estimates would clearly increase for multiple node traversals.

Theories of the excitation of the solar p modes by turbulence favour the localization of such phenomena in the outermost layers of the convection zone, where the Mach number of the convective motions is peaked (e.g., Goldreich & Kumar 1990). As noted previously, while the relative importance of the contributions from the various multipole terms is still an open issue, all attain greater efficiency at higher Mach numbers. Further, the observation of individual seismic events as down-drafts in the cool, inter-granular lanes (Rimmele et al. 1995; Espagnet et al. 1996; Goode et al. 1998) favours a location for the source in the upper several-hundred kilometers of the convection zone. When we bring this independent information to bear, we are inclined to favour the extracted source locations indicated by Figs. 3 and 4 as opposed to those obtained by moving deeper into the cavity by one (or more) nodes.

5.2 Fitting the VIRGO/SPM spectrum for the correlated noise component

5.2.1 Size of the correlated component

As noted in Section 2, we assume that the presence of a correlated component, α_{corel}, in the intensity observations is responsible for altering the resonant profiles sufficiently to reverse the negative asymmetries seen in the Doppler-velocity data. Resonant peaks in the VIRGO/SPM spectrum must therefore be fitted to a model of the form indicated by Equation 6.

First, we attempted to fit for d_s and α_{corel} simultaneously in the VIRGO/SPM spectrum . We adopted the same fitting strategy outlined in Section 5.1, but with the following modifications:

(i) The continuous coverage provided by the VIRGO/SPM data negated the need to include temporal sidebands in the fitting model.
(ii) A single, real (as opposed to complex) parameter describing α_{corel} – assumed to be constant over the mode-pair fitting range – was optimized.
(iii) And the fixed, m-component height ratios were modified so as to be appropriate to the full-disc filter of the intensity observations.

We immediately found that the fitting ran into difficulties. In order to reverse the asymmetries (i.e., with respect to those observed in the BiSON data), the minimization routines displayed a clear preference for setting the best-fit α_{corel} to zero, achieving the reversal by simply moving the source far enough inside the cavity to pass through another node (e.g., see Fig. 2). The returned best-fit values for d_s were consequently somewhat deeper than those implied from the BiSON analysis, with the disparity increasing at lower n (where the cavity-node separation is larger). Under the requirement that we return similar estimated source depths for both datasets, this is clearly unsatisfactory.

We therefore adopted the strategy of fixing the relative source depths, d_s, on input, according to the best-fit BiSON values. We used a simple, two-part, straight-line parameterization of the best-fit d_s values shown in Fig. 3 (as derived from fits to a model generated from G_Ψ). In Fig. 5, we show the values for $\alpha_{\rm corel}$ (Equation 6) extracted by fitting the VIRGO/SPM blue-channel spectrum in this manner. (The plotted error bars are the formal uncertainties from the Hessian of each fit.) Each plotted datum corresponds to that fraction of the maximum value of the Green's function G_Ψ that is needed to bring about the required reversal in asymmetry between the velocity and intensity data. We verified the robustness of the results by performing a series of Monte Carlo simulations, as outlined for the source-depth analysis in Section 5.1 – however, this time we also added varying degrees of correlated noise to the input profiles.

The magnitude of $\alpha_{\rm corel}$ – of the order of a few per cent over the n range fitted here – increases in the wings of the p-mode spectrum, where the fractional asymmetry of the modes is larger. This is illustrated in Fig. 6. Here, we have fitted a polynomial skew-symmetric formalism – as derived by Nigam & Kosovichev (1998) – to $l = 2/0$ modes in both the VIRGO/SPM (blue) and BiSON spectra. (For a description of the use of this fitting formalism with low-l data, see Toutain et al. 1998; Chaplin et al. 1999.) The effects of skew symmetry appear explicitly as a single parameter in the formalism. Fitted estimates of the parameter provide a measure of the fractional asymmetry in the modes, as plotted in the figure (triangles from fits to the VIRGO/SPM blue dataset, crosses from fits to the BiSON dataset). Clearly, greater changes are required to the shape of the observed resonances at low and high n in order to give the required reversals in skewness. To achieve this, the modifying influence, and therefore the size, of $\alpha_{\rm corel}$ must be increased. We also note that the negligible size of the fitted $\alpha_{\rm corel}$ at $n = 15$ (off the scale in Fig. 5) is consistent with the out-of-line negative fractional skewness shown in Fig. 6.

While $\alpha_{\rm corel}$ indicates that fraction of the normalized Green's function that is required to give the necessary asymmetry reversal, $A_{\rm corel}$ – defined according to Equation 7 – takes into account the frequency dependence of the mode amplitudes, and as such serves as a measure of the "effective" amplitude of correlated granular component. This we plot in Fig. 7, together with the fitted radial ($l = 0$) p-mode amplitudes which were used to determine each $A_{\rm corel}$ (data again plotted for the blue channel).

Here, $A_{\rm corel}$ decreases in magnitude with increasing radial order n. This behaviour can be reasoned from the following, naive argument. The power spectrum of intensity fluctuations arising from the granulation follows a Kolmogorov scaling with eddy size (Komm, Mattig & Nesis 1990), i.e., more power is observed at larger spatial scales. Since larger-scale eddies couple more-strongly to modes with lower frequencies in the excitation process (e.g., Osaki 1990; Chang & Gough 1998), we might expect the size of the imprinted, granular component to show a general decrease with increasing n.

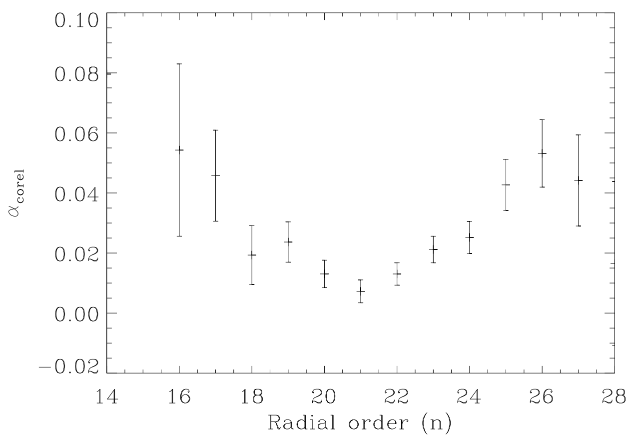

Figure 5. Fitted $\alpha_{\rm corel}$ extracted from the analysis of the VIRGO/SPM blue-channel spectrum. Each datum corresponds to that fraction of the maximum value of the Green's function that is required to give the required asymmetry reversal in the intensity data. The plotted error bars are the formal uncertainties from the Hessian of each fit.

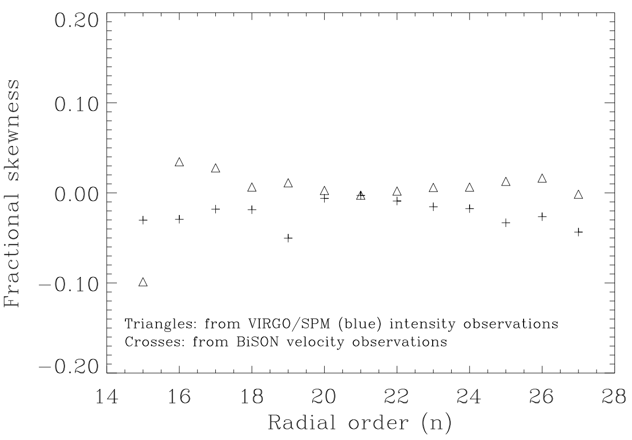

Figure 6. Fractional asymmetries of radial modes extracted by fitting a polynomial skew-symmetric formalism – as derived by Nigam & Kosovichev (1998) – to modes in both the VIRGO/SPM blue (triangles) and BiSON (crosses) spectra.

In addition, we have converted our fitted $\alpha_{\rm corel}$ to the (dimensionless) β' of Kumar & Basu (1999a), which also provides a measure of the effective magnitude of the correlated signal. This parameter is defined according to the product of: the ratio of the amplitude of the flux variation of a convective eddy to that of the oscillation it excites; and a factor related to the height above the base of the photosphere at which the observations are made. Our inferred values of β' from the SPM blue-channel spectrum decrease from ~ 0.8 at $n = 16$ to ~ 0.15 at $n = 27$, displaying a similar variation as a function of n to that shown by $A_{\rm corel}$. These values are similar to those calculated from a solar model by Kumar & Basu. Further, these authors show that

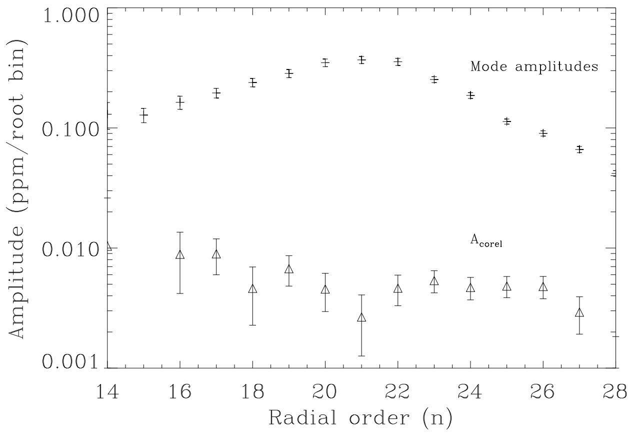

Figure 7. The effective amplitude of the correlated signal, $A_{\rm corel}$, as inferred from the analysis of the blue-channel VIRGO/SPM spectrum. Each $A_{\rm corel}$ (plotted triangles) is calculated by multiplying the fitted $\alpha_{\rm corel}$ by the fitted p-mode amplitude, $A_{\rm I}$ at each n. Here, we show results for the radial ($l = 0$) modes. The plotted error bars are determined from the elements of the Hessian matrix of each fit.

given similar depths of excitation and a fixed observation height, $\beta^{'}$ should decrease with increasing radial order n. The levelling-off of the downward trend at high n in our inferred values of $\beta^{'}$ and $A_{\rm corel}$ probably reflects the decreasing absolute source depth shown in Fig. 4 (which in turn arises from the lack of any marked variation in d_s at $n > 20$).

At this point, it is again worth noting that we neglected to take into account the phase relationship between the eddy and mode – as considered by Kumar & Basu – and as such fitted only for the effective magnitude of the correlated component by including a real, rather than complex, variable in our analyses (although, of course, it was added to the elements of G_Ψ in a complex manner).

5.2.2 The correlated component at different wavelengths

We also fitted for the correlated component in an intensity spectrum generated from data collected at red wavelengths by the VIRGO/SPM photometers. Over the range $16 \leq n \leq 26$, we find that the mean $A_{\rm corel}$ is a factor 1.36 ± 0.14 larger at blue compared to red wavelengths. The ratio is at least in the correct sense if one seeks an explanation in terms of the height in the atmosphere at which the observation is made. Here, we pre-suppose that the red-channel data are less affected by the granulation, since they are sensitive to changes some ~ 10 km above the base of the photosphere; the effective observation height for the blue channel is ~ 0 km. (We have used the analyses of Solanki & Unruh (1997) to determine these for the separate channels of the SPM.) However, since the amplitudes of the radial acoustic modes are much lower at red wavelengths (by a factor of ~ 2.5), the modifying influence of the measured $A_{\rm corel}$ is greater, and therefore the observed mode profiles are more (positively) skew-symmetric. In fact, we find that the fitted $\alpha_{\rm corel}$ are, on average, some 1.85 ± 0.17 times larger in the red channel.

The range of effective heights of observation covered by the channels of the SPM are quite narrow. Tests of the height dependence of $A_{\rm corel}$ can be extended by making intensity observations in the core of suitable spectral lines. We would expect to see the influence of the granular component decrease for observations made higher up in the photosphere (or at the bottom of the chromosphere). Observations of the intensity fluctuations in the photosphere arising from convective overshoot indicate that both the magnitude and the degree of coherence of the signal, compared to that observed at the top of the convection zone, fall off quite noticeably in the first ~ 100 km or so (e.g., Komm, Mattig & Nesis 1990; Espagnet et al. 1995). Further, the degree of coherence of smaller-scale structures (which relate to convection) appears to be destroyed at smaller heights in the photosphere. If we were to compare intensity observations of the acoustic modes made in a suitable line core, with those made here in the continuum by the VIRGO/SPM, we might therefore expect to see: (i) less-positive levels of skew symmetry in the line-core profiles, owing to the reduced influence of the granular component; and (ii) a greater reduction of the positive skewness at higher frequencies in the line-core data, where the modes couple more strongly to smaller-scale eddy structures, whose convective "signature" is destroyed at lower levels in the photosphere.

6 SUMMARY

We have used the solutions to a simple, one-dimensional wave equation – which is intended to describe the essential elements of the solar resonant acoustic cavity – as formalistic models to which to fit low-l modes in observational helioseismic power spectra. These come from the Green's function, G_Ψ, of the equation. The models allow for the modifying influence of a correlated component of the solar granulation on the observed shape of the resonant p-mode profiles. We have analyzed independent spectra, generated from observations of the oscillations made in both velocity (by BiSON) and intensity (by the VIRGO/SPM photometers on board SOHO) in a complementary fashion.

The location of the excitation source with respect to the bounded cavity appears explicitly in the fitting formalism. When the mode profiles are characterized by G_Ψ, our analysis places the source in the outer layers of the convection zone, with a mean position some 221 ± 17 km beneath the base of the photosphere. We also find that the source lies above the upper turning point of the bounded cavity for mode overtone numbers (n) of less than ≈ 16. With the profiles defined according to the first derivative of the Green's function, dG_Ψ/dr (i.e., characterizing a different multipole source), we recover source depths of the order of ~ -1500 km. We note here that a source characterized by a suitable admixture of G_Ψ and dG_Ψ/dr can admit solutions that are shallower than those returned by fitting G_Ψ alone – we intend to address the issue of mixed-parity source types in a forthcoming paper.

Under the premise that it is only the intensity observations that are modified to any appreciable degree by the the correlated granular motion, we find that the fractional amplitude of this component – at blue wavelengths – with respect to that of the radial ($l = 0$) p modes increases from about 2 per cent near the centre of the spectrum, to ≈ 5

per cent at the extreme n fitted here (15 and 27 respectively). The absolute amplitude of the component decreases with increasing n, and is found to be smaller at red (compared to blue) wavelengths. However, since the red-channel mode amplitudes are somewhat lower, the modifying influence of the correlated signal is greater, and as a result the red-channel mode profiles display higher levels of positive skew symmetry.

ACKNOWLEDGMENTS

This work utilizes data collected by the VIRGO instrument on board the SOHO satellite, and the ground-based Birmingham Solar-Oscillations Network (BiSON). We would like to thank the members of both teams for allowing us to use these data. SOHO is a project of international cooperation between ESA and NASA. BiSON is funded by the UK Particle Physics and Astronomy Research Council. WJC acknowledges the support of an ESA Internal Fellowship. We thank Takashi Sekii for providing the modelled solar acoustic potential.

REFERENCES

Abrams D. & Kumar P., 1996, ApJ, 472, 882
Appourchaux T., Chaplin, W. J., Elsworth, Y., Isaak, G. R., McLeod, C. P., Miller, B. A. & New, R., 1998, in: Proc. IAU Symp. 185 'New Eyes to See inside the Sun and Stars. Pushing the Limits of Helio- and Asteroseismology with New Observations from Ground and from Space', ed. Deubner F.-L., Kluwer, Dordrecht, p. 45
Chang H.-Y. & Gough D. O., 1998, Sol. Phys., 181, 251
Chaplin W. J., Elsworth Y., Isaak G. R., Lines R., McLeod C. P., Miller B. A. & New R., 1998, MNRAS, 300, 1077
Chaplin W. J., Elsworth Y., Isaak G. R., Miller B. A. & New R., 1999, MNRAS, in press
Christensen-Dalsgaard J., 1989, MNRAS, 239, 977
Christensen-Dalsgaard J., et al., 1996, Science, 272, 1286
Christensen-Dalsgaard J., Rabello-Soares M. C., Rosenthal C. S. & Thompson M. J., in 'SOHO6/GONG98 Workshop: Structure and dynamics of the interior of the Sun and Sun-like stars', eds. Korzennik S. & Wilson A., ESA SP-418, p. 147
Duvall T. L., Jefferies S. M., Harvey J. W., Osaki Y. & Pomerantz M. A., 1993, ApJ, 410, 829
Espagnet O., Muller R., Roudier Th., Mein N. & Mein P., 1995, A&ASS, 109, 79
Espagnet O., Muller R., Roudier Th., Mein N., Mein P. & Malherbe J. M., 1996, A&A, 313, 297
Fröhlich C. et al., 1997a, Sol. Phys., 170, 1
Fröhlich C. et al., 1997b, Sol. Phys., 170, 267
Gabriel M., 1995, A&A, 302, 271
Goldreich P. & Kumar P., 1990, ApJ, 363, 694
Goode P. R., Strous L. H., Rimmele T. R. & Stebbins R. T., 1998, ApJ, 495, L27
Komm R., Mattig W. & Nesis A., 1990, A&A, 239, 340
Korzennik S. G., 1998, in 'SOHO6/GONG98 Workshop: Structure and dynamics of the interior of the Sun and Sun-like stars', eds. Korzennik S. & Wilson A., ESA SP-418, p. 933
Kumar P. & Basu S., 1999a, ApJ, submitted (LANL pre-print astro-ph/9808144 v2)
Kumar P. & Basu S., 1999b, ApJ, submitted (LANL pre-print astro-ph/9808143 v2)
Lighthill M. J., 1952, Proc. Roy. Soc. London A., 211, 564
Nigam R., Kosovichev A. G., Scherrer P. H. & Schou J., 1998, ApJ, 495, L115
Nigam R. & Kosovichev A. G., 1998, ApJ, 505, L51
Osaki Y., 1990, in: Progress of Seismology of the Sun and Stars, p. 145, eds. Osaki Y. & Shibahashi H., Springer-Verlag, Berlin
Press W. H., Teukolsky S. A., Vetterling W. T. & Flannery B. P., 1992, in: Numerical Recipes in Fortran (Second Edition), Cambridge University Press, Cambridge, p. 407
Rast M. P. & Bogdan T. J., 1997, ApJ, 496, 527
Rhodes E. J. Jr., Kosovichev A. G., Schou J., Scherrer P. H. & Reiter J., 1997, Sol. Phys., 175, 287
Rimmele T. R., Goode P. R., Harold E. & Stebbins R. T., 1995, ApJ, 444, L119
Rosenthal C. S., 1998a, ApJ, 508, 864
Rosenthal C. S., 1998b, in 'SOHO6/GONG98 Workshop: Structure and dynamics of the interior of the Sun and Sun-like stars', eds. Korzennik S. & Wilson A., ESA SP-418, p. 957
Roxburgh I. W. & Vorontsov S. V., 1997, MNRAS, 292, L33
Solanki S. K. & Unruh Y. C., 1997, A&A, 329, 747
Stein R. F. & Nordlund A., 1998, ApJ, 499, 914
Toutain T. & Appourchaux T., 1994, A&A, 289, 649
Toutain T., et al., 1997a, Sol. Phys., 175, 311
Toutain T., Appourchaux T., Fröhlich C., Kosovichev A. G., Nigam R. & Scherrer P. H., 1998, ApJ, 506, L147